

Mechanism analysis of nanofiltration membrane fouling behavior by mixed BSA–HA using AFM with modified polyamide–probe

Fang Gao^{a,b,c}, Yuxing Sheng^{a,b,*}, Yuping Li^{a,b}, Hongbin Cao^{a,b}, Chunlei Su^{a,b,d}

^aNational key Laboratory of Biochemical Engineering, Institute of Process Engineering, Chinese Academy of Sciences, Beijing, 100190, China, Tel./Fax: +86-10-82544844; emails: 232230204@qq.com (F. Gao), yxsheng@home.ipe.ac.cn (Y. Sheng), stringsplay@126.com (Y. Li), 564355246@qq.com (C. Su), Tel./Fax: +86-10-82544839; email: hbcao@home.ipe.ac.cn (H. Cao)

^bKey Laboratory of Green Process and Engineering, Institute of Process Engineering, Chinese Academy of Sciences, Beijing, 100190, China, Tel./Fax: +86-10-82544844; emails: 232230204@qq.com (F. Gao), yxsheng@home.ipe.ac.cn (Y. Sheng), stringsplay@126.com (Y. Li), 564355246@qq.com (C. Su), Tel./Fax: +86-10-82544839; email: hbcao@home.ipe.ac.cn (H. Cao)

^cUniversity of Chinese Academy of Sciences, Beijing, 100190, China, Tel./Fax: +86-10-82544844; email: 232230204@qq.com (F. Gao)

^dUniversity of Xiangtan, Xiangtan, 411105, China, Tel./Fax: +86-10-82544844; 564355246@qq.com (C. Su)

Received 29 March 2016; Accepted 22 June 2016

ABSTRACT

In this work, fouling mechanisms of mixed foulants, that is, bovine serum albumin (BSA) and humic acid (HA), on nanofiltration (NF) under different factors, including pH, ionic strength, and Ca^{2+} , were investigated by using atomic force microscopy (AFM). Considering that fouling behavior mainly appeared at the polyamide (PA) separation layer of NF membrane, AFM probes modified with PA which was the dominating material of effective separation layer, and coating $[\text{BSA-HA}]_n$ were prepared. Fouling mechanisms of mixed foulants on the NF membrane were studied through measurements of the interfacial forces of $[\text{BSA-HA}]_n$ -PA membrane and $[\text{BSA-HA}]_n$ - $[\text{BSA-HA}]_n$. Fouling experiments with $[\text{BSA-HA}]_n$ were carried out using PA membrane, and the results indicated severe flux reduction occurring at low pH, thereby decreasing the ionic strength or adding Ca^{2+} . The fouling behavior of NF membrane was determined by the interfacial forces (F/R) of $[\text{BSA-HA}]_n$ -PA and $[\text{BSA-HA}]_n$ - $[\text{BSA-HA}]_n$, thus both forces were measured. Results showed that the forces of $[\text{BSA-HA}]_n$ -PA membrane were stronger than those of $[\text{BSA-HA}]_n$ - $[\text{BSA-HA}]_n$. Moreover, both forces were enhanced with low pH, ionic strength and added Ca^{2+} . Results verified that the F/R of $[\text{BSA-HA}]_n$ -PA membrane determined the cake formation occurrence time, and F/R of $[\text{BSA-HA}]_n$ - $[\text{BSA-HA}]_n$ maintained a linear correlation with fouling degree.

Keywords: Nanofiltration; Polyamide membrane; Fouling mechanism; Modified PA probe; Mixed foulants

1. Introduction

Nanofiltration (NF) membrane has been presently used in a wide range of applications, including water purification, wastewater reclamation, and seawater desalination. Of particular interest is the use of NF membranes in advanced wastewater reclamation

to augment limited available water supply [1–3]. Unfortunately, the efficient application of NF membrane technology is significantly hindered by organic fouling because wastewater effluent contains a considerable amount of organic substances. Fouling behavior results in not only water flux reduction, and compromised permeate quality. Fouling can be affected by many different factors, such as feed water composition, solution chemistry, and membrane properties [4,5]. Therefore, the mechanisms dominating organic fouling, which are as considerable practical significance for sustainable application of NF membrane technology, should be thoroughly understood.

*Corresponding author.

Organic foulants contain proteins, organic acids, and polysaccharides in regular effluent [6]. Solution chemistry has remarkable effect on fouling behavior, because of the changing interaction between foulants, and foulant–membrane. For example, Tang et al. [7] investigated the effect of pH and calcium ions on NF membrane fouling behavior by using humic acid (HA). They found that HA accumulation on membrane surfaces increased with low pH, due to the electric interaction among organic molecules. In addition, interspecies forces can be affected by ionic strength, and they are reduced with increasing ionic strength [8]. Previous investigations played significance on revealing the fouling behavior during NF process, but they focused mainly on single organic foulant. However, the actual feed typically contains mixed foulants rather than a single foulant, thus work for mixed foulants should be given attention [9–11].

Studies on fouling behavior for non-porous membrane illustrated that foulant cake layer on the membrane surface plays a dominant role on membrane fouling [5,12]. Furthermore, foulant deposition rate and cake thickness are determined via interspecies forces [13]. Therefore, analysis of interactions between foulant–foulant and foulants–membrane is a key in the field of membrane fouling behavior [14,15]. Taking into account the carboxyl-rich characteristics of organic substances, Elimelech et al. [16–18] investigated the interaction forces between the foulant and virgin or fouled membrane surface using a carboxylic modified colloidal probe. They also elucidated that interfacial forces are correlated directly with fouling rate and chemical cleaning performance. Kimura et al. [19] used hydroxyl- and carboxyl-modified microspheres to compare the adhesion forces between microspheres and a polyvinylidene fluoride (PVDF) or a polyethylene (PE) membrane, respectively. The use of a modified probe provides accurate assessment of the interaction forces when the colloidal probe made of materials similar to membranes has a confluent of model foulants. Subsequently, Wang and Meng et al. [20,21] further elaborated the organic fouling behavior of PVDF ultrafiltration (UF) membranes, via self-made PVDF colloidal probes coated with different foulants, such as bovine serum albumin (BSA) and HA. The focus used in studies about adhesion forces have turned from forces of single foulant toward to those of mixed foulant. For example, Miao et al. [22] investigated the effect of mixed foulants, including sodium alginate (SA)/HA on the fouling behavior of a PVDF UF membrane by using the PVDF and foulant-coated probes, respectively. As mentioned above, the material modifying AFM probes is forced on PVDF, which fabricates mainly UF membrane. The separation layers of the majority of NF and reverse osmosis (RO) membranes were consisted of a thin layer of polyamide (PA) [23–25]. The interaction between mixed foulants and this layer plays a dominant role on the fouling behavior. Nonetheless, studies on the interactions between mixed foulant and PA membrane under variant solution chemistries are rare.

Therefore, in the present study, a PA colloidal probe was assembled via PA microsphere on the end of a cantilever. Mixed foulant BSA-HA coated colloidal probe was also prepared through adsorbing BSA-HA on the surface of PA microsphere. The study aimed to investigate the adhesion

forces between [BSA-HA]_n-PA membrane and [BSA-HA]_n-[BSA-HA]_n via a self-made PA colloidal probe under variant solution chemistries (pH, ionic strength, and divalent cation). Simultaneously, the influence of the corresponding solution chemistry on membrane fouling behavior was investigated. Results of AFM force measurements, which were accompanied with structure and composition of foulant cake on the PA membrane, provided novel insights into the membrane organic fouling process in the reuse of wastewater in complex systems.

2. Materials and methods

2.1. Model organic foulant and PA membrane

HA (Sigma-Aldrich 53680) and BSA (Sigma-Aldrich A1933, ≥98% purity) were used as model protein and organic acid foulants and stored at 4°C in the dark. All reagents and chemicals were of analytical grade with purity over 99%, unless otherwise specified. Ultrapure water (Milli-Q, resistivity of 18.2 MΩ) was used to prepare the working solutions. The membrane investigated in this study was a highly antifouling, thin-film composite NF, and its surface composition was composed of aromatic PA.

2.2. Preparation of colloidal probe

The colloidal probe used in intermolecular force measurements was prepared via a PA microsphere onto a commercial V-shaped SiN tipless AFM cantilever end (NP-10; Bruker, Germany) with a spring constant of 0.35 N/m. For the fabrication of PA membrane material probe, the following instructions were followed: a micromanipulator was used to first coat the free end of the cantilever, by using a small amount of glue with the aid of a scanning electron microscope (SEM). Subsequently, a ~5 μm diameter of self-produced PA microsphere was fixed to the end of the cantilever. The cantilever with the PA microsphere was then placed in air for ~30 min. Moreover, the prepared colloidal probes were stored at room temperature for at least 24 h prior to measurement. For the preparation of foulant-coated probe: a PA colloidal probe was completely immersed into the solution, which included BSA and HA by AFM, until the mixed foulants adsorbed on the microsphere to form a layer of foulants. Fig. 1 shows SEM images of a PA colloidal probe and [BSA-HA]_n-probe constructed using the above method. To confirm the applications of [BSA-HA]_n-probe constructed using the above method, virgin PA membrane, PA microspheres and [BSA-HA]_n-coated microspheres were characterized through FTIR, as shown in Fig. 2. The spring constant of PA colloidal probe was measured by using the thermal fluctuation method.

2.3. Membrane characterization

Membrane surface morphology of virgin and fouled PA membranes was measured on by using SEM (JSM-7610F, JEOL Ltd., Japan) to determine the structure of the filter cake, and how variant properties influence the filter cake caused by HA combined with BSA. All samples were completely dried in clean plastic boxes at room temperature.

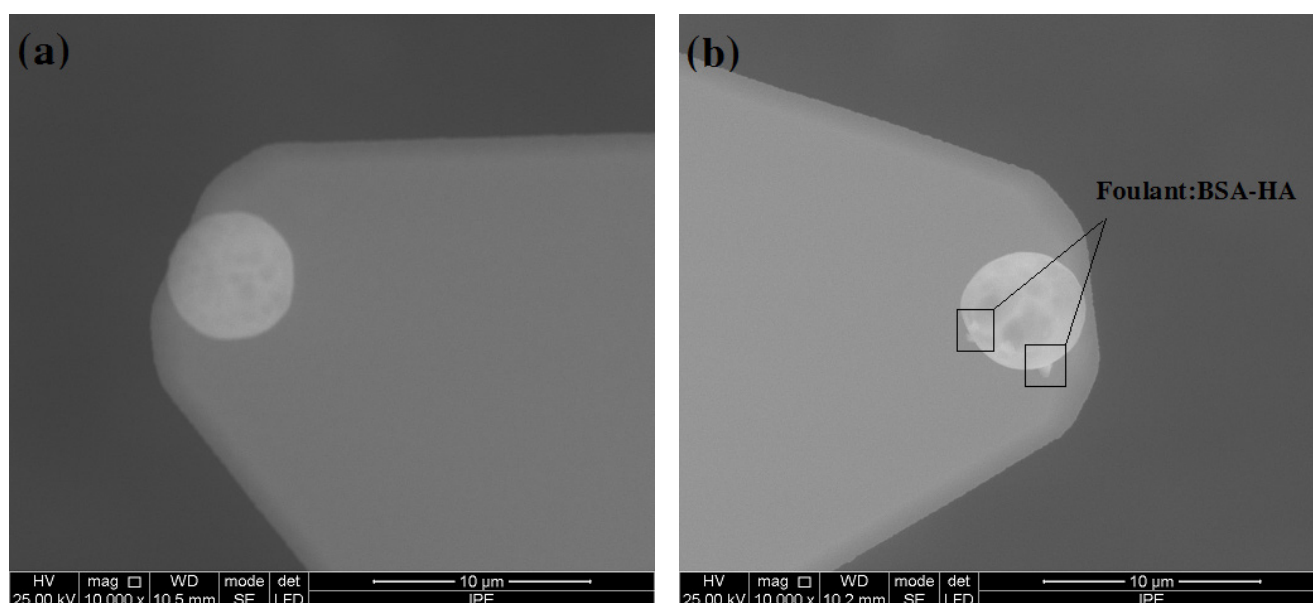


Fig. 1. SEM image of: (a) PA colloidal AFM probe; (b) $[\text{BSA-HA}]_n$ -probe.

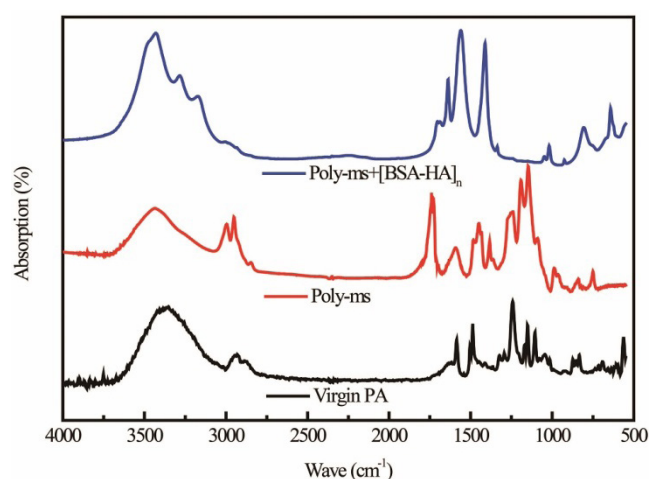


Fig. 2. FTIR image of virgin PA membrane, PA colloids and $[\text{BSA-HA}]_n$ -coated PA colloids.

The surface elemental composition of virgin and fouled PA membranes was measured with a X-ray photoelectron spectrometer (XPS, ESCALAB 250Xi, Thermo Fisher Scientific Inc., U.S.) equipped with a monochromatic $\text{Al K}\alpha$ X-ray source ($h\nu$ 1486.7 eV) incident at 90° relative to the axis of a hemispherical energy analyzer.

2.4. Interfacial force measurements

After each fouling experiment, the fouled membrane was transferred in a solution identical to that used in the corresponding fouling experiment. The forces between colloidal probe and fouled membrane were measured in a fluid cell filled with test solution via AFM (FASTSCAN, Bruker, Germany). Force measurements were first carried out with a PA colloidal probe, which was used as a PA membrane to

investigate the adhesion force of $[\text{BSA-HA}]_n$ -PA membrane. Subsequently, the foulant-coated PA colloidal probe was used as foulant to determine the $[\text{BSA-HA}]_n$ - $[\text{BSA-HA}]_n$ adhesion force. All AFM measurements were carried out in corresponding test solution in contact mode. A fouled membrane sample was mounted in the bottom of the fluid cell, and the fluid cell was filled with the test solution. For each type of membrane sample, force measurements were performed at five different locations, and more than 20 force curves were obtained at each location.

2.5. Membrane filtration experiments

Membrane fouling experiments were carried out in a laboratory scale cross-flow membrane filtration system consisting of a rectangular membrane cell. The test membranes were kept in ultrapure water and the water was replaced weekly. For each filtration experience, a virgin membrane was immersed in ultrapure water until loading into the test cell. The membrane was first compacted by the pure water for at least 2 h until the permeate flux became stable before the fouling test. Each filtration test contained the mixed organic fouling system and continued about 20 h until the desired permeate flux loss was observed. The pH of all feed solutions was adjusted with 1 M NaOH or HCl solution. Unless specified otherwise, the following conditions were optimized: total foulant concentration of 20 mg/L (10 mg/L BSA + 10 mg/L HA); applied pressure 500 kPa; crossflow velocity 0.1 m/s; and temperature 20°C .

3. Results and discussion

To elucidate the mixed foulant mechanisms of antifouling NF membrane, the effects of solution properties (pH, ionic strength and Ca^{2+}) on the fouling behavior of membrane through mixed organic foulants were investigated. The foulant constituents on membrane

surface and the fouled membrane surface were measured. Furthermore, the adhesion forces of $[\text{BSA-HA}]_n$ -PA membrane and $[\text{BSA-HA}]_n$ - $[\text{BSA-HA}]_n$ were measured at the corresponding test solution.

3.1. Membrane fouling experiments

3.1.1. Effect of pH on membrane fouling behavior

The effect of solution pH on the fouling behavior by mixed organic BSA+HA system is shown in Fig. 3. Within a pH range of 7–10, the flux decline rates were barely observed in the initial filtration stage (3 h), whereas the fouling behavior at pH 7 became gradual and had 24% decline at 20 h. On the contrary, when the solution pH was 4, the flux decline rate was more dramatic than others at the initial stage of fouling test, and the ultimate permeate flux was only 55% of the initial value (J/J_0). The changing trend of fouling behavior with solution pH was similar to those reported in the studies for single foulant system [26,27].

3.1.2. Effect of ionic strength on membrane fouling behavior

For mixed foulants aggregation was also influenced by the ion strength in the feed. Fig. 4 shows the effect of ionic strength on membrane fouling behavior at pH 7. Severer fouling was observed at low ionic strength. For example, at ionic strength of 10 mM, the flux over 20 h of fouling test was lower than 76% of the initial flux. When ionic strength was 50 mM, the flux reduction was around 20% at the same period of the fouling test. With the ionic strength increasing continuously to 200 mM, the flux decline in the early phase of fouling test was not obvious. Moreover, the flux decline rate tended to decrease further, and flux loss over 20 h was only 7%.

3.1.3. Effect of calcium ion on membrane fouling behavior

Calcium ion influence was further studied by comparing the presence/absence of Ca^{2+} in the feeds. According to

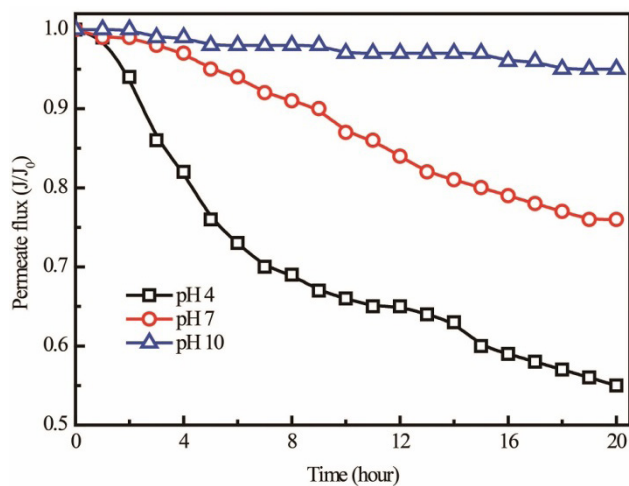


Fig. 3. Effect of pH on flux decline curves for $[\text{BSA-HA}]_n$. Experimental conditions: mass concentrations of BSA and HA, 10 + 10 mg/L; ionic strength, 10 mM NaCl.

Fig. 5, the flux decline rate with 1 mM Ca^{2+} was more severe than that with 0 mM Ca^{2+} at initial stage. In addition, the decline rate with 1 mM Ca^{2+} within the filtration period of 15–20 h was invariable. Relatively, the rate without Ca^{2+} became gradually slight at the same period. Ca^{2+} ions not only form a complex among BSA–HA aggregates with the carboxylic functional groups, but also alleviate the electrostatic repulsive forces between foulants and the membrane surface [9,28].

3.2. Characterization of membrane and foulants

Comprising smooth morphological surface of virgin PA membrane, morphological changes of fouled membranes at different conditions were observed in the SEM images according to Fig. 6. As parts (b–d) of Fig. 6 shown, BSA–HA deposited layer on PA membrane at pH 4 was tighter and denser than those in neutral and alkaline conditions, which

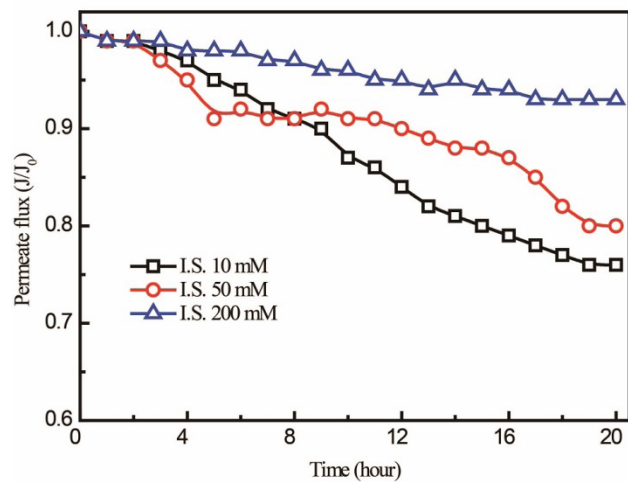


Fig. 4. Effect of ionic strength on flux decline curves for $[\text{BSA-HA}]_n$. Experimental conditions: mass concentrations of BSA and HA, 10 + 10 mg/L; pH 7.

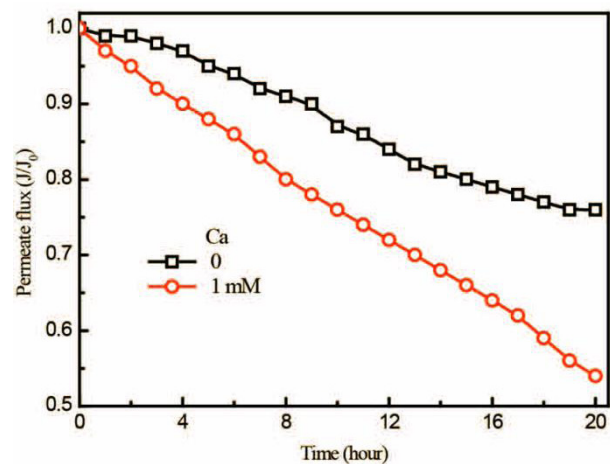


Fig. 5. Effect of Ca^{2+} on flux decline curves for $[\text{BSA-HA}]_n$. Experimental conditions: mass concentrations of BSA and HA, 10 + 10 mg/L; ionic strength 10 mM; pH 7.

may be attributed to the variant polymeric structures of BSA–HA with the changing solution pH. For example, the membrane surface covered by the foulants was relatively smooth; because of the loose gel layer formed on the membrane surface at pH 10. Considering the influence of inorganic salt, when the ionic strength increased in the feed, the fouling gel transformed from cake to crystalloid, and the organic foulants were distributed on the membrane surface in parts c, e, and f of Fig. 6. When the feed contained Ca^{2+} ions, homogenous sheet crystal occurred and led to flux reduction, in addition to heterogeneous organic crystal. For BSA–HA mixed system, the formation of organic fouling cake can play a dominant role on the decline of permeate flux. Moreover, the surfaces of PA membranes deposited BSA–HA in different levels, and this deposition behavior was closely related to the solution pH, ionic strength and Ca^{2+} .

Table 1 presents the XPS results quantifying the elemental composition (C, N, O, and S) of the separation

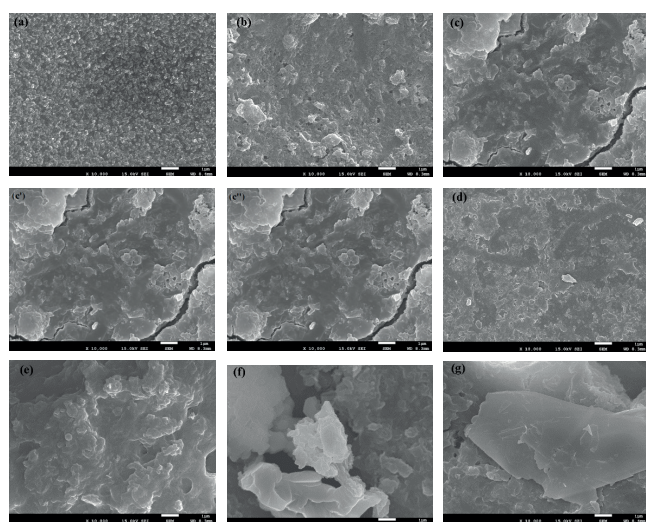


Fig. 6. SEM images of the virgin and fouled membranes under variant conditions: (a) virgin PA, (b) pH 4, (c) pH 7, (c') 10 mM, (c'') absence of Ca^{2+} , (d) pH 10, (e) 50 mM, (f) 200 mM, (g) presence of Ca^{2+} .

Table 1
XPS survey and high resolution scans for virgin and fouled PA membranes under variant conditions

	Atomic fraction (%)			
	C	N	O	S
Virgin PA	69.22	11.79	18.74	0.26
Fouled PA				
pH 4	64.24	12.04	22.62	1.09
pH 7*	62.93	8.3	28.37	0.5
pH 10	58.01	7.97	33.56	0.46
I.S. 50 mM	61.94	4.94	31.89	1.23
I.S. 200 mM	62.26	7.04	30.07	0.64
Ca^{2+}	65.5	8.59	24.42	1.48

*P.S. pH 7 also represents the following test conditions: ionic strength 10 mM or the absence of Ca^{2+} .

layer on virgin PA membrane and foulant layers in fouled samples. The elemental content in the virgin PA composite membrane was as follows: C: 69.22%, N: 11.79%, O: 18.74%, and S: 0.26%. The sulfur elements might come from the substrate layer made of polysulfone [29]. The changing atomic fraction of C, N, and O is attributed to the fractions of foulants adsorbed on the membrane surface [30]. Furthermore, the atomic fraction of S on the membrane was determinant of mixed foulant composition, which was attributed to the only source of sulfur element provided by disulfide bond among BSA micromoles [8,25]. As shown in Table 1, the atomic fractions of C, N, and S decreased, nor increased atomic fraction of O with increasing solution pH. The results may testify that $[\text{BSA-HA}]_n$ fouling layer on the PA membrane contained a large amount of BSA molecules at low pH (pH 4), and the additional amount of HA molecules can be deposited on the PA membrane at pH 7 and 10. Considering that HA molecule is constituted amount of hydroxyl and carboxyl groups, this molecules possesses low hydroxyl, carboxyl and ester groups comparing with BSA molecular structure [31,32]. In addition to solution pH, the effect of ionic strength and the presence of calcium ions on elements fractions on the fouled PA membrane is shown in Table 1. When ionic strength increased from 10 mM (test condition: pH 7) to 200 mM, the atomic fractions of O and S were enhanced to some extent, which resulted from the weakened electrostatic repulsion between $[\text{BSA-HA}]_n$ and the membrane via the electrical double layer compression [13]. However, the reducing electrostatic interaction between BSA and HA with increasing ionic strength can contribute to the slack fouling cake on the PA membrane surface. An increasing S fraction on the membrane with Ca^{2+} addition in the feed illustrated that $[\text{BSA-HA}]_n$ on the membrane surface contained more BSA molecules than that in the absence of Ca^{2+} . This phenomenon can be explained by the following several reasons: (a) the BSA–BSA chelating complex formed by Ca^{2+} , and (b) the bridge interaction between BSA and membrane [12,33].

3.3. Interfacial adhesion force

AFM interaction force measurement is an adopted technique for the measurement of the interaction force between membrane and foulant. The normalized adhesion force (F/R) serves as an indicator for the fouling propensity of polymeric membranes. The adhesion forces of $[\text{BSA-HA}]_n$ –virgin PA membrane and $[\text{BSA-HA}]_n$ – $[\text{BSA-HA}]_n$ at variant conditions (pH, ionic strength and Ca^{2+}) were quantified.

3.3.1. Interfacial adhesion force of $[\text{BSA-HA}]_n$ –PA membrane

For fouling behavior during NF process, interfacial adhesion force between foulants $[\text{BSA-HA}]_n$ and PA membrane revealed the fouling degree (flux reduction rate) at the initial stage, considering that deposited mass of foulants on the PA membrane surface was determined through the adhesion force of $[\text{BSA-HA}]_n$ and virgin PA membrane. Therefore, the representative adhesion force–distance curves and frequency distributions of $[\text{BSA-HA}]_n$ –

virgin PA affected by solution pH, ionic strength and with Ca^{2+} are presented in Fig. 7. Parts a and b of Fig. 7 depict the effect of pH on the adhesion forces between $[\text{BSA-HA}]_n$ and virgin PA, as follows: pH 4 (1.7 mN/m) > pH 7 (0.7 mN/m) > pH 10 (0.3 mN/m). Considering the results of the flux decline of three pH values, the stronger force was well recognized to signify more severe fouling as shown in Figs. 3 and 6(b)–(d). The reasons could be explained the changing zeta potential values of foulants and PA. At pH 4, the electrostatic attractive forces between foulants and virgin PA may contribute to the adhesion forces between them. With the increase of pH, the electrostatic repulsion between foulants and PA was enhanced, due to the negative charge of both in central and alkaline conditions [21]. Moreover, the adhesion forces between $[\text{BSA-HA}]_n$ –virgin PA were

measured at 10, 50, and 200 mM NaCl solutions at pH 7, and parts c and d of Fig. 7 show adhesion forces vs. separation distance and frequencies of F/R of the three types ionic strength were 0.7, 0.6, and 0.3 mN/m. The results can be contradictory to precious studies that the effect of double layer compression generally leads to an overall reduction in the electrostatic repulsive force among foulants with increasing ionic strength [7,26,34]. Among heterogeneous molecules, the contributions of large charge density should not be neglected, and electric screening and increasing of Debye radius between foulants and groups of virgin PA can weaken adhesion forces at high salt concentration [35,36]. According to above discussions, molecular interactions between mixed foulants and membrane, along with ion electric screening, which can affect the interfacial adhesion

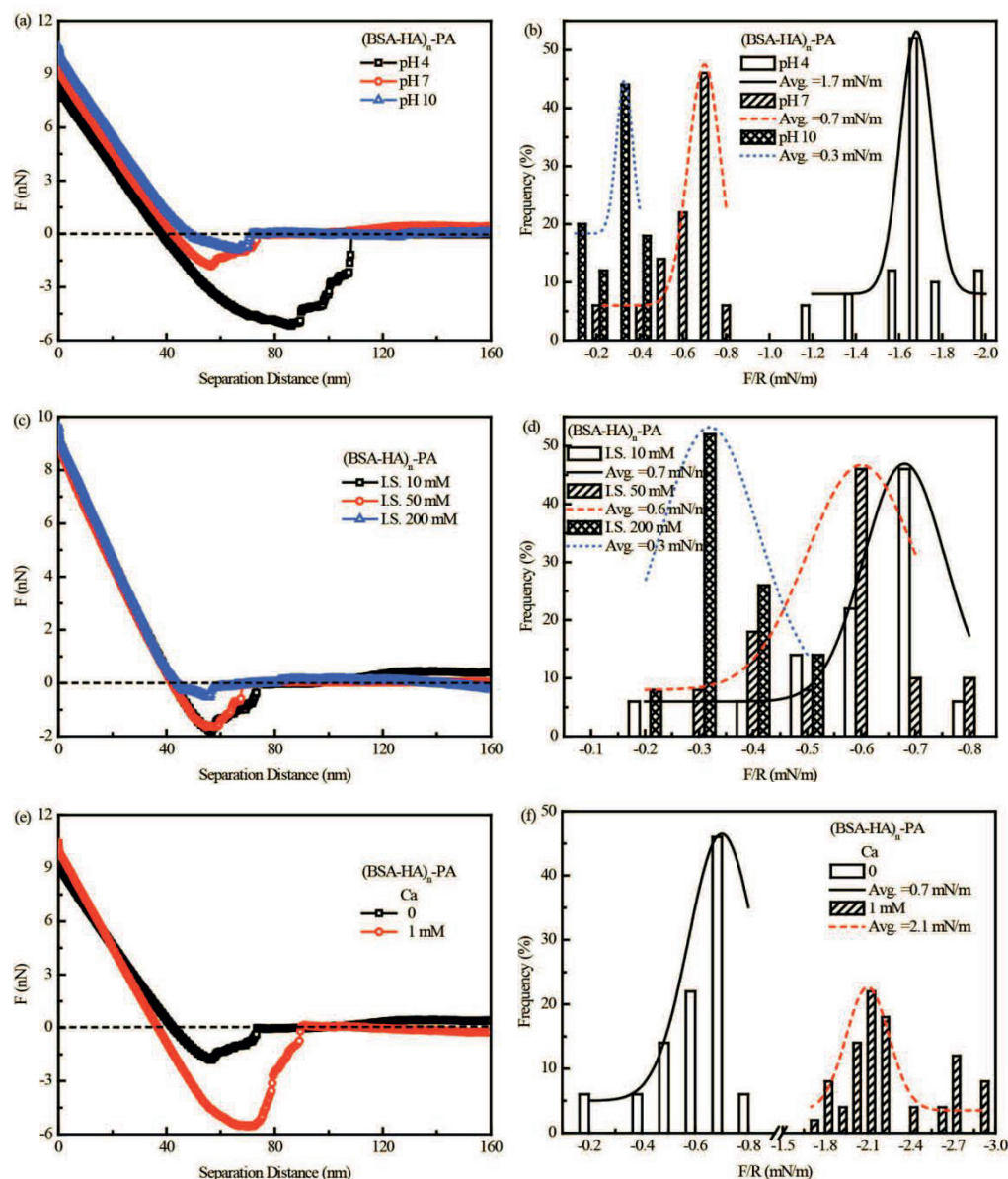


Fig. 7. Representative force vs. distance curves and the frequency distributions of foulant–virgin PA, (a and b) pH, (b–d) ionic strength, and (e and f) the presence or absence of Ca^{2+} .

forces of $[\text{BSA-HA}]_n$ -virgin PA, were susceptible to polyvalent cations. Therefore, when Ca^{2+} ions were added in the feed, the F/R of $[\text{BSA-HA}]_n$ and virgin PA with Ca^{2+} soared to 2.1 mN/m, which was threefold more than those without Ca^{2+} , as shown in parts e and f of Fig. 7. This result was attributed to that Ca^{2+} ions exceeded electrostatic repulsion and provided interfacial energy between foulants and PA surface [37,38].

3.3.2. Interfacial adhesion force of $[\text{BSA-HA}]_n$ - $[\text{BSA-HA}]_n$

Considering the formation of fouling cake through $[\text{BSA-HA}]_n$ adsorbed on the PA membrane surface, the adhesion forces of $[\text{BSA-HA}]_n$ - $[\text{BSA-HA}]_n$ can not only determine the formation and size of $[\text{BSA-HA}]_n$ in the

feed, but also identify the fouling degree at the late stage of fouling test. As shown in part a and b of Fig. 8, the forces of $[\text{BSA-HA}]_n$ - $[\text{BSA-HA}]_n$ were 0.5, 0.4, and 0.2 mN/m, respectively, which were attributed to the strong electric repulsive forces in $[\text{BSA-HA}]_n$. With the increasing solution pH, the zeta potential values of polymers $[\text{BSA-HA}]_n$ and fouled membrane surface declined rapidly. Additionally, the strengthening electric repulsion weakened their adhesion forces, because of their large number of dissociative carboxyl groups. The average polymerization degree of $[\text{BSA-HA}]_n$ is vulnerable to inorganic salt. Thus, the adhesion forces of $[\text{BSA-HA}]_n$ - $[\text{BSA-HA}]_n$ at corresponding ionic strength were measured. The F/R was also reduced with adding ionic strength according to parts c and d of Fig. 8. The results illustrated that an increasing dissolved

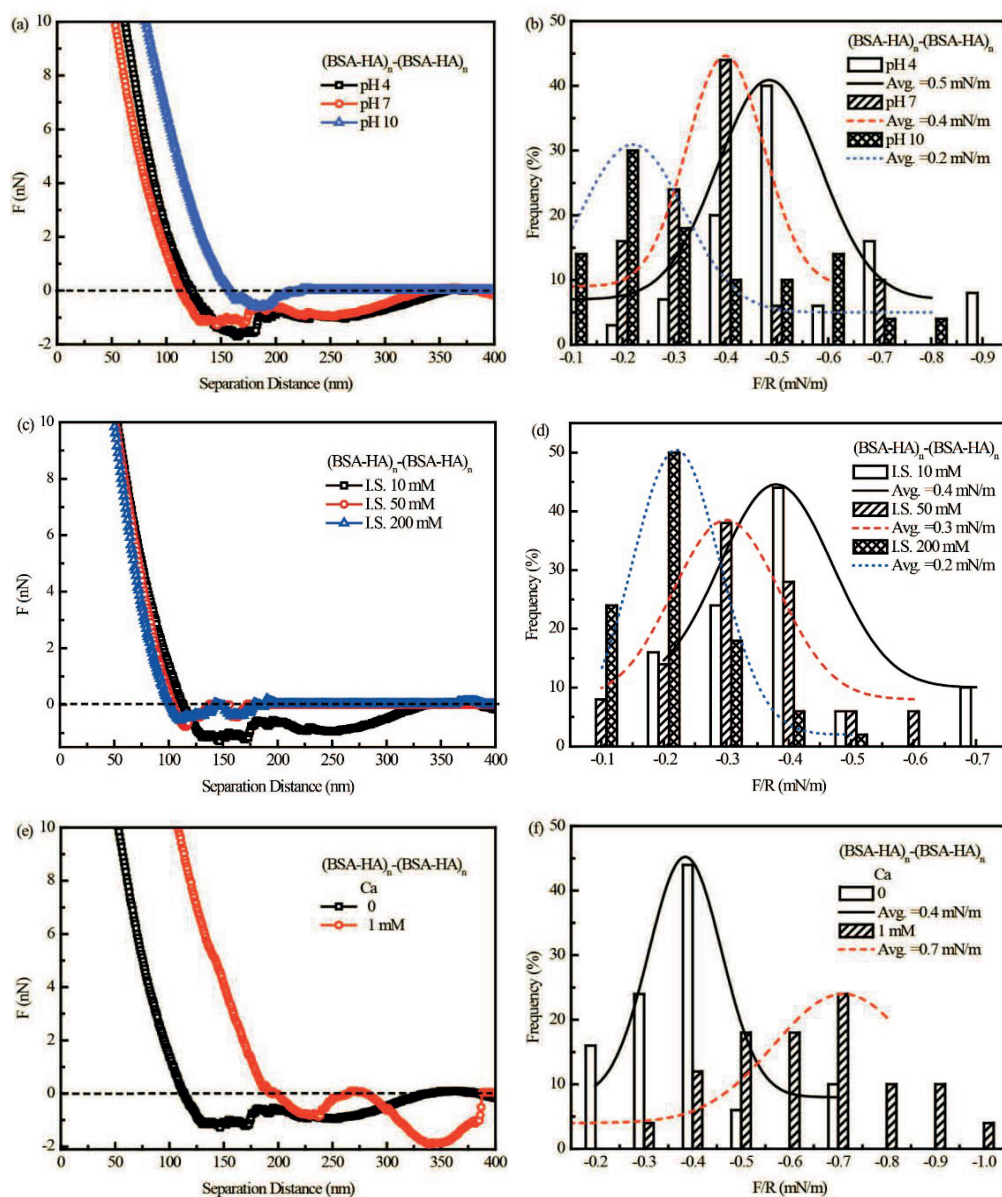


Fig. 8. Representative force vs. distance curves and the frequency distributions of foulant-foulant, (a and b) pH, (b–d) ionic strength, and (e and f) the presence or absence of Ca^{2+} .

salt concentration was a disadvantage to aggregation of charged substances, yet to the adsorption of organic foulants on fouled membrane surface, because of Debye screening theory. When the ionic strength was enhanced in the feed, the Debye screening length among foulants (or between foulants and fouled membrane) increased, thereby hindering the interfacial forces. Furthermore, when the feed contained Ca^{2+} ions, parts e and f of Fig. 8 show that the F/R of $[\text{BSA-HA}]_n$ - $[\text{BSA-HA}]_n$ in the presence of Ca^{2+} was 0.7 mN/m, and the value was higher without Ca^{2+} . These results can elucidate that Ca^{2+} ions represented an attractive interaction among BSA-HA and promoted the formation of larger-sized $[\text{BSA-HA}]_n$ via increasing the hydrophobic effect of foulants [33].

3.4. The correlation between adhesion force and membrane fouling behavior

The permeate flux decline reflected the interfacial force of membrane-foulant, and the fouling degree mainly coming from the cake formation on the membrane surface was determined via the adhesion force of foulant-foulant [39–41]. Therefore, the interaction forces of $[\text{BSA-HA}]_n$ -PA membrane and $[\text{BSA-HA}]_n$ - $[\text{BSA-HA}]_n$ studied under different chemical properties were also compared.

Table 2 shows, all that, the F/R of $[\text{BSA-HA}]_n$ -PA membrane and $[\text{BSA-HA}]_n$ - $[\text{BSA-HA}]_n$ weakened with increasing pH value. Moreover, the F/R of $[\text{BSA-HA}]_n$ - $[\text{BSA-HA}]_n$ was weaker than that of $[\text{BSA-HA}]_n$ -PA at corresponding pH. This observation was in agreement with the previous studies of Wang and Meng et al. [21,35]. The results are in well accordance with the permeate flux decline under three types of pH. A large number of amino, carboxylic and phenolic functional groups were included in both foulants and PA membrane surface. At low pH (~4), a significant portion of carboxylic and phenolic groups became protonated, thereby causing a reduced charge density of the BSA-HA molecules and thus a significant reduction in foulant-foulant electrostatic interaction [26,34]. This phenomenon may significantly destabilize the BSA-HA suspension [13,42]. Furthermore, the mass of foulants adsorbed on the membrane was

partly promoted by the electrostatic attraction of $[\text{BSA-HA}]_n$ and PA membrane surface [43], which was followed by aggravated roughness of membrane surface and ultimately led to tight fouling cake [10]. With the increasing pH value, the electrostatic repulsive forces both $[\text{BSA-HA}]_n$ and PA membrane were enhanced, and the $[\text{BSA-HA}]_n$ molecules hindered effectively foulants deposition on the membrane surface. At alkaline condition, in addition to strengthening of the above mentioned repulsions, the electric charges of both BSA and HA molecules were negative, and the repulsive forces between BSA and HA may originally impede the progress of BSA and HA coacervation. For the influence of inorganic salt concentration on F/R, the F/R of $[\text{BSA-HA}]_n$ -PA membrane decreased with increasing ionic strength, which may be attributed to the suppressive interaction among foulants, and between mixed foulants and PA membrane because of electrostatic screening [35]. The F/R measurements of $[\text{BSA-HA}]_n$ - $[\text{BSA-HA}]_n$ presented a similar trend. Nevertheless, the electric repulsive force of homogeneous substances with their same charge becomes less due to the electrical double layer compression, which consequently contributes to adhesion force [36,44]. Relatively, for heterogeneous substances, the interaction between distinctive groups, that is, amino and carboxylic groups, also weakened. This observation can be explained by the reduction of the F/R of $[\text{BSA-HA}]_n$ -PA membrane with enhanced ionic strength [11,35]. Additionally, a similar condition occurred at interfacial affection between BSA and HA. In the feed, without Ca^{2+} ions, the main bridging effects between BSA and HA were hydrogen bonding interaction and acid-based group interaction, including the amino of BSA molecules and carboxylate or carbonyl of HA molecules. When Ca^{2+} ions were present in the feed solution, the F/R of both $[\text{BSA-HA}]_n$ -PA membrane and $[\text{BSA-HA}]_n$ - $[\text{BSA-HA}]_n$ significantly increased, which was probably caused by the binding of their Ca^{2+} -carboxylate complex between foulants and PA membrane (foulants) [16,45,46]. Consequently, the increasing F/R among foulants can reduce the electrostatic repulsion between aggregation monomers BSA-HA and promote the formation of polymers $[\text{BSA-HA}]_n$. Increasing F/R between foulants and membrane can also overcome the energy barrier of foulants adsorbing on hydrophilic surface of PA membrane, and thus enhancing the deposition rate of polymers $[\text{BSA-HA}]_n$ on the membrane surface [20,47].

Considering that adhesion forces of $[\text{BSA-HA}]_n$ -PA membrane can have a determined role on the adsorption rate of foulants on the membrane, the occurrence time of obvious flux reduction during the filtration process was identified. The flux did not decline sharply until the permeate flux declined to 0.97 of initial flux according to Figs. 3–5. The results may suggest an entire cake formation on the membrane surface until this time. Therefore, the ratio of normalized flux remained at 0.97 and the corresponding test time had a linear correlation with the F/R of $[\text{BSA-HA}]_n$ -PA membrane under variant conditions as part a of Fig. 9 shown. In addition, the F/R of $[\text{BSA-HA}]_n$ - $[\text{BSA-HA}]_n$ can not only present the aggregation capacity among foulants, but also determine the flux reduction degree with cake accumulation [21] over long period of fouling test. Part b of Fig. 9 illustrates that a linear correlation had been analyzed between F/R of $[\text{BSA-HA}]_n$ - $[\text{BSA-HA}]_n$ and ultimate flux over 20 h. The modified AFM probe technique reflects the

Table 2
Adhesion forces (F/R) of $[\text{BSA-HA}]_n$ -PA membrane and $[\text{BSA-HA}]_n$ - $[\text{BSA-HA}]_n$ under variant conditions

	F/R (mN/m)	
	$[\text{BSA-HA}]_n$ -PA membrane	$[\text{BSA-HA}]_n$ - $[\text{BSA-HA}]_n$
pH 4	1.7	0.5
pH 7	0.7	0.4
pH 10	0.3	0.2
I.S. 10 mM	0.7	0.4
I.S. 50 mM	0.6	0.3
I.S. 200 mM	0.3	0.2
0 mM Ca^{2+}	0.7	0.4
1 mM Ca^{2+}	2.1	0.7

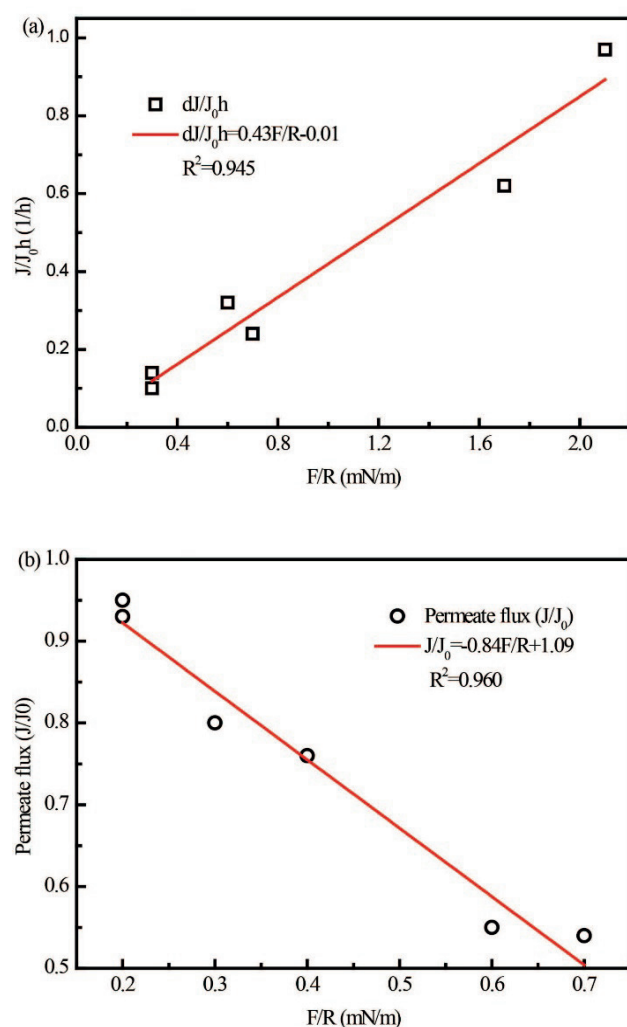


Fig. 9. Adhesion forces (F/R) and normalized permeate flux under different conditions: (a) forces of foulant–PA membrane and initial flux reduction; (b) forces of foulant–foulant and ultimate flux.

particular interfacial property of membrane under variant conditions, that is, pH, ionic strength and polyvalent cation. Thus, the technique can predict fouling behavior of mixed foulants on NF membrane, to some extent, disregarding the influence of different chemical properties on foulants and NF membrane.

4. Conclusion

In this study, the PA membrane material probe was assembled. Moreover, the corresponding mixed foulants [BSA-HA]_n were successfully adsorbed on the surface of PA colloidal probe and formed the [BSA-HA]_n-coating probe. The effects of mixed foulants on the antifouling NF membrane fouling behavior were systematically investigated under different conditions. The results indicated the following: (1) both forces decreased with an increasing of pH; (2) both forces increased with decreasing

ionic strength; and (3) the forces were enhanced significantly in the presence of Ca²⁺. The adhesion forces of [BSA-HA]_n-virgin PA membrane were stronger than those between [BSA-HA]_n-[BSA-HA]_n at the same condition. In addition, the cake formation occurrence had a linear correlation with interfacial forces of [BSA-HA]_n-PA membrane. The adhesion forces of [BSA-HA]_n-[BSA-HA]_n had a linear correlation with the flux reduction over a long test period. Therefore, the results predict the time of cake formation and fouling behavior on the PA NF membrane of mixed foulants via measurements of both forces.

References

- [1] N. Fridman-Bishop, O. Nir, O. Lahav, V. Freger, Predicting the rejection of major seawater ions by spiral-wound nanofiltration membranes, *Environ. Sci. Technol.*, 49 (2015) 8631–8638.
- [2] B. Su, T. Wu, Z. Li, X. Cong, X. Gao, C. Gao, Pilot study of seawater nanofiltration softening technology based on integrated membrane system, *Desalination*, 368 (2015) 193–201.
- [3] A.H.M.A. Sadmani, R.C. Andrews, D.M. Bagley, Impact of natural water colloids and cations on the rejection of pharmaceutically active and endocrine disrupting compounds by nanofiltration, *J. Membr. Sci.*, 450 (2014) 272–281.
- [4] T.O. Mahlangu, J.M. Thwala, B.B. Mamba, A. D’Haese, A.R.D. Verliefde, Factors governing combined fouling by organic and colloidal foulants in cross-flow nanofiltration, *J. Membr. Sci.*, 491 (2015) 53–62.
- [5] G. Feng, H. Chu, B. Dong, Fouling effects of algogenic organic matters during nanofiltration of naproxen, *Desalination*, 350 (2014) 69–78.
- [6] M. Mänttari, L. Puro, J. Nuortila-Jokinen, M. Nyström, Fouling effects of polysaccharides and humic acid in nanofiltration, *J. Membr. Sci.*, 165 (2000) 1–17.
- [7] C.Y. Tang, Y.N. Kwon, J.O. Leckie, Fouling of reverse osmosis and nanofiltration membranes by humic acid—Effects of solution composition and hydrodynamic conditions, *J. Membr. Sci.*, 290 (2007) 86–94.
- [8] A.W. Seng, E. Menachem, Protein (BSA) fouling of reverse osmosis membranes: implications for wastewater reclamation, *J. Membr. Sci.*, 296 (2007) 83–92.
- [9] A.M. Comerton, R.C. Andrews, D.M. Bagley, The influence of natural organic matter and cations on fouled nanofiltration membrane effective molecular weight cut-off, *J. Membr. Sci.*, 327 (2009) 155–163.
- [10] A.E. Contreras, A. Kim, Q. Li, Combined fouling of nanofiltration membranes: mechanisms and effect of organic matter, *J. Membr. Sci.*, 327 (2009) 87–95.
- [11] Y.-N. Wang, C.Y. Tang, Protein fouling of nanofiltration, reverse osmosis, and ultrafiltration membranes—The role of hydrodynamic conditions, solution chemistry, and membrane properties, *J. Membr. Sci.*, 376 (2011) 275–282.
- [12] F. Zhao, K. Xu, H. Ren, L. Ding, J. Geng, Y. Zhang, Combined effects of organic matter and calcium on biofouling of nanofiltration membranes, *J. Membr. Sci.*, 486 (2015) 177–188.
- [13] C.Y. Tang, Y.-N. Kwon, J.O. Leckie, The role of foulant–foulant electrostatic interaction on limiting flux for RO and NF membranes during humic acid fouling—Theoretical basis, experimental evidence, and AFM interaction force measurement, *J. Membr. Sci.*, 326 (2009) 526–532.
- [14] D.J. Johnson, S.A.A. Malek, B.A.M. Al-Rashdi, N. Hilal, Atomic force microscopy of nanofiltration membranes: effect of imaging mode and environment, *J. Membr. Sci.*, 389 (2012) 486–498.
- [15] J. Stawikowska, A.G. Livingston, Assessment of atomic force microscopy for characterisation of nanofiltration membranes, *J. Membr. Sci.*, 425–426 (2013) 58–70.
- [16] Q. Li, M. Elimelech, Organic fouling and chemical cleaning of nanofiltration membranes: measurements and mechanisms, *Environ. Sci. Technol.*, 38 (2004) 4683–4693.

- [17] S. Lee, M. Elimelech, Relating organic fouling of reverse osmosis membranes to intermolecular adhesion forces, *Environ. Sci. Technol.*, 40 (2006) 980–987.
- [18] W.S. Ang, S. Lee, M. Elimelech, Chemical and physical aspects of cleaning of organic-fouled reverse osmosis membranes, *J. Membr. Sci.*, 272 (2006) 198–210.
- [19] H. Yamamura, K. Kimura, T. Okajima, H. Tokumoto, Y. Watanabe, Affinity of functional groups for membrane surfaces: implications for physically irreversible fouling, *Environ. Sci. Technol.*, 42 (2008) 5310–5315.
- [20] L. Wang, R. Miao, X. Wang, Y. Lv, X. Meng, Y. Yang, D. Huang, L. Feng, Z. Liu, K. Ju, Fouling behavior of typical organic foulants in polyvinylidene fluoride ultrafiltration membranes: characterization from microforces, *Environ. Sci. Technol.*, 47 (2013) 3708–3714.
- [21] X. Meng, W. Tang, L. Wang, X. Wang, D. Huang, H. Chen, N. Zhang, Mechanism analysis of membrane fouling behavior by humic acid using atomic force microscopy: effect of solution pH and hydrophilicity of PVDF ultrafiltration membrane interface, *J. Membr. Sci.*, 487 (2015) 180–188.
- [22] R. Miao, L. Wang, X. Wang, Y. Lv, Z. Gao, N. Mi, T. Liu, Preparation of a polyvinylidene fluoride membrane material probe and its application in membrane fouling research, *Desalination*, 357 (2015) 171–177.
- [23] R. Zhang, W. Shi, S. Yu, W. Wang, Z. Zhang, B. Zhang, L. Li, X. Bao, Influence of salts, anion polyacrylamide and crude oil on nanofiltration membrane fouling during desalination process of polymer flooding produced water, *Desalination*, 373 (2015) 27–37.
- [24] Y. Jin, Y. Ju, H. Lee, S. Hong, Fouling potential evaluation by cake fouling index: theoretical development, measurements, and its implications for fouling mechanisms, *J. Membr. Sci.*, 490 (2015) 57–64.
- [25] Y.-N. Wang, C.Y. Tang, Fouling of nanofiltration, reverse osmosis, and ultrafiltration membranes by protein mixtures: the role of inter-foulant-species interaction, *Environ. Sci. Technol.*, 45 (2011) 6373–6379.
- [26] K.L. Jones, C.R. O'Melia, Protein and humic acid adsorption onto hydrophilic membrane surfaces: effects of pH and ionic strength, *J. Membr. Sci.*, 165 (2000) 31–46.
- [27] Q. She, C.Y. Tang, Y.-N. Wang, Z. Zhang, The role of hydrodynamic conditions and solution chemistry on protein fouling during ultrafiltration, *Desalination*, 249 (2009) 1079–1087.
- [28] P.v.d. Brink, A. Zwijnenburg, G. Smith, H. Temmink, M.v. Loosdrecht, Effect of free calcium concentration and ionic strength on alginate fouling in cross-flow membrane filtration, *J. Membr. Sci.*, 345 (2009) 207–216.
- [29] L. Jin, W. Shi, S. Yu, X. Yi, N. Sun, C. Ma, Y. Liu, Preparation and characterization of a novel PA-SiO₂ nanofiltration membrane for raw water treatment, *Desalination*, 298 (2012) 34–41.
- [30] M.A. Sari, S. Chellam, Surface water nanofiltration incorporating (electro) coagulation–microfiltration pretreatment: fouling control and membrane characterization, *J. Membr. Sci.*, 437 (2013) 249–256.
- [31] A.S. Gorzalski, O. Coronell, Fouling of nanofiltration membranes in full- and bench-scale systems treating groundwater containing silica, *J. Membr. Sci.*, 468 (2014) 349–359.
- [32] Y. Li, Y. Su, X. Zhao, R. Zhang, J. Zhao, X. Fan, Z. Jiang, Surface fluorination of polyamide nanofiltration membrane for enhanced antifouling property, *J. Membr. Sci.*, 455 (2014) 15–23.
- [33] T. Lin, Z.J. Lu, C. Wei, Interaction mechanisms of humic acid combined with calcium ions on membrane fouling at different conditions in an ultrafiltration system, *Desalination*, 357 (2015) 26–35.
- [34] H. Mo, K.G. Tay, H.Y. Ng, Fouling of reverse osmosis membrane by protein (BSA): effects of pH, calcium, magnesium, ionic strength and temperature, *J. Membr. Sci.*, 315 (2008) 28–35.
- [35] Y.-N. Wang, C.Y. Tang, Nanofiltration membrane fouling by oppositely charged macromolecules: investigation on flux behavior, foulant mass deposition, and solute rejection, *Environ. Sci. Technol.*, 45 (2011) 8941–8947.
- [36] R. Chan, V. Chen, The effects of electrolyte concentration and pH on protein aggregation and deposition: critical flux and constant flux membrane filtration, *J. Membr. Sci.*, 185 (2001) 177–192.
- [37] H.-J. Butt, B. Cappella, M. Kappl, Force measurements with the atomic force microscope: technique, interpretation and applications, *Surf. Sci. Rep.*, 59 (2005) 1–152.
- [38] W.S. Ang, M. Elimelech, Fatty acid fouling of reverse osmosis membranes: implications for wastewater reclamation, *Water Res.*, 42 (2008) 4393–4403.
- [39] K. Kimura, Y. Hane, Y. Watanabe, G. Amy, N. Ohkuma, Irreversible membrane fouling during ultrafiltration of surface water, *Water Res.*, 38 (2004) 3431–3441.
- [40] S. Lee, J. Cho, M. Elimelech, Combined influence of natural organic matter (NOM) and colloidal particles on nanofiltration membrane fouling, *J. Membr. Sci.*, 262 (2005) 27–41.
- [41] E.M.V. Hoek, M. Elimelech, Cake-enhanced concentration polarization: a new fouling mechanism for salt-rejecting membranes, *Environ. Sci. Technol.*, 37 (2003) 5581–5589.
- [42] S. Hong, M. Elimelech, Chemical and physical aspects of natural organic matter (NOM) fouling of nanofiltration membranes, *J. Membr. Sci.*, 132 (1997) 159–181.
- [43] D. Nanda, K.-L. Tung, Y.-L. Li, N.-J. Lin, C.-J. Chuang, Effect of pH on membrane morphology, fouling potential, and filtration performance of nanofiltration membrane for water softening, *J. Membr. Sci.*, 349 (2010) 411–420.
- [44] M. Nilsson, G. Trägårdh, K. Östergren, The influence of pH, salt and temperature on nanofiltration performance, *J. Membr. Sci.*, 312 (2008) 97–106.
- [45] M. Herzberg, S. Kang, M. Elimelech, Role of Extracellular polymeric substances (EPS) in biofouling of reverse osmosis membranes, *Environ. Sci. Technol.*, 43 (2009) 4393–4398.
- [46] B. Mi, M. Elimelech, Chemical and physical aspects of organic fouling of forward osmosis membranes, *J. Membr. Sci.*, 320 (2008) 292–302.
- [47] H. Susanto, M. Ulbricht, Influence of ultrafiltration membrane characteristics on adsorptive fouling with dextrans, *J. Membr. Sci.*, 266 (2005) 132–142.